# Seeded and unseeded high-order parametric down-conversion

Cameron Okoth,[1,2,*] Andrea Cavanna,[1,2] Nicolas Y. Joly,[2,1] and Maria V. Chekhova[1,2,3]
[1]*Max Planck Institute for the Science of Light, Staudtstraße 2, 91058 Erlangen, Germany*
[2]*Institute of Optics, Information and Photonics, University of Erlangen-Nürnberg, Staudtstraße 7/B2, 91058 Erlangen, Germany*
[3]*Department of Physics, M. V. Lomonosov Moscow State University, Leninskie Gory, 119991 Moscow, Russia*

(Received 26 November 2018; published 9 April 2019)

Spontaneous parametric down-conversion (SPDC) has been one of the foremost tools in quantum optics for over five decades. Over that time, it has been used to demonstrate some of the curious features that arise from quantum mechanics. Despite the success of SPDC, its higher-order analogs have never been observed, even though it has been suggested that they generate far more unique and exotic states than SPDC. An example of this is the emergence of non-Gaussian states without the need for postselection. Here we calculate the expected rate of emission for *n*th-order SPDC with and without external stimulation (seeding). Focusing primarily on third-order parametric down-conversion, we estimate the photon detection rates in a rutile crystal for both the unseeded and seeded regimes.

DOI: 10.1103/PhysRevA.99.043809

## I. INTRODUCTION

Nonlinear optical effects are so far the most convenient tool for generating nonclassical states of light. For instance, parametric down-conversion [1–3] and four-wave mixing [4] are widely used for producing photon pairs, single photons (through heralding [5,6]), quadrature squeezed light [7], and twin beams [8]. Meanwhile, there are attempts to realize higher-order nonlinear effects, leading to the generation of photon triplets (or third-order squeezing [9–11]). Despite a large number of proposals and theoretical papers [12–17], the direct decay of a pump photon into three daughter photons, further called third-order parametric down-conversion (TOPDC), has not yet been realized experimentally. Photon triplet states have indeed been obtained in experiment using cascaded quadratic nonlinear effects [18] or accidentally overlapping photon pairs emitted through parametric down-conversion [19]. However, the statistics of light emitted through these effects is very different from the statistics of photons being generated by TOPDC: for instance, in the "cascaded" experimental realizations, there is a strong asymmetry between the photon numbers in the three output beams. Recently, rather high rates of photon triplet generation have been reported by using exciton and biexciton transitions in coupled quantum dots [20], but it is not clear to what extent this process is similar to TOPDC. One of the standout features of TOPDC that sets it apart from the aforementioned processes is that it forms a non-Gaussian state. Non-Gaussian processes are highly sought after due to their application in quantum computing [21].

As opposed to third-harmonic generation, an effect that only involves the interaction of single-mode strong classical fields, the reverse process TOPDC couples a continuum of weak vacuum fields where the number of modes is limited by the phase-matching condition. This is general for all orders of parametric down-conversion.

Due to the receding value of the nonlinear susceptibility, higher orders of spontaneous parametric down-conversion (SPDC) suffer from weaker and weaker efficiencies. It is one of the primary explanations as to why TOPDC has not been reported yet, as opposed to second-order SPDC which is routinely observed. A natural step towards the observation of TOPDC is to seed (stimulate) the emission of one of the photons in the three-photon state. An important breakthrough in this direction has been made in Ref. [22] where two seeding beams were used. However, no nontrivial photon statistics could be observed at the output in this case.

In this paper, we give a general description of *n*th-order SPDC and compare the efficencies of lower-order processes and higher-order processes. We then describe how the seeding of a *n*th-order process using a strong coherent source affects the rate of photon emission and changes the fundamental properties of the emitted radiation. In particular, we show that seeded TOPDC generates a two-photon state and not a three-photon state, such as spontaneous TOPDC. Despite the loss of the three-photon state, we still believe stimulated TOPDC is an interesting effect to observe as it can be used as a way to study spontaneous TOPDC, the same way as stimulated emission tomography [23] is used to characterize the properties of SPDC.

The paper is structured as follows. In Sec. II, we derive the rate of *n*-photon SPDC starting from Fermi's golden rule. In Sec. III, we analyze the phase-matching function and distinguish between two regimes: broadband detection and narrow-band detection. In Sec. IV, we relate the emission rates of high-order processes to the emission rates of lower-order processes. The effect of seeding is considered in Sec. V, and the spectral properties of seeded and unseeded TOPDC emission are explored in Secs. VI and VII. In Sec. VIII, we present an estimate for the expected triplet-, double-, and single-photon count rates for seeded and unseeded TOPDC

*cameron.okoth@mpl.mpg.de

 

in rutile. We conclude (Sec. IX) with a discussion of the main results.

## II. THE RATE OF A *n*-PHOTON TRANSITION PER MODE

A $n$th-order parametric down-conversion process involves the transition of a single pump photon to a state of $n$ photons occupying, in the general case, $n$ modes. Using the approach outlined in Ref. [24], we calculate the rate of a $n$-photon transition per mode using Fermi's golden rule,

$$\Gamma^{(n)} = \frac{2\pi}{\hbar^2}|\langle\langle 1||_n \hat{H}^{(n)}||0\rangle\rangle_n|^2 \delta(\Delta\omega^{(n)}), \tag{1}$$

where

$$\Delta\omega^{(n)} = \omega_p - \sum_{i=1}^{n}\omega_i, \tag{2}$$

the subscript $i$ denotes the mode with frequency $\omega_i$ and wave-vector $\vec{k}_i$, the subscript $p$ denotes the pump mode, and $||0\rangle\rangle_n$, $||1\rangle\rangle_n$ signify the $n$-dimensional vacuum state and the product state of $n$ modes each populated by a single photon, respectively. Starting from the electric dipole Hamiltonian [24,25]: $\hat{H} = -\vec{d}\cdot\vec{E}$, integrating over all dipole moments for the macroscopic Hamiltonian and taking all nonlinear terms of the resulting expression we can write $\hat{H}^{(n)}$, the Hamiltonian of a $n$th-order nonlinear perturbation, in an isotropic medium as

$$\hat{H}^{(n)} = -\epsilon_0 \frac{n!\chi^{(n)}}{2^n}\int F(\vec{r})E_p^{(+)}(\vec{r})\prod_{i=1}^{n}E_i^{(-)}(\vec{r})d^3\vec{r} + \text{H.c.}, \tag{3}$$

where $\epsilon_0$ is the vacuum permittivity, $\chi^{(n)}(\vec{r})$ is the $n$th-order susceptibility, which has been separated into the effective susceptibility $\chi^{(n)}$ and its spatial distribution $F(\vec{r})$, a function that is dimensionless and takes a maximum value of unity. $E_i^{(+/-)}(\vec{r})$ is the positive or negative frequency electric-field component of the $i$th mode. The pump field $E_p^{(+)}(\vec{r})$, using the correspondence principle, can be described classically in the limit of large photon numbers. Assuming that the pump propagates in the $z$ direction, the classical and quantized electric fields are

$$E_p^{(+)}(\vec{r}) = A_p(x,y)\sqrt{\frac{2I_p}{\epsilon_0 c n_p}}e^{\imath k_p z},$$
$$E_i^{(-)}(\vec{r}) = \sqrt{c_i}a_i^{\dagger}e^{-\imath\vec{k}_i\cdot\vec{r}}, \tag{4}$$

respectively. Here,

$$c_i = -\frac{\hbar\omega_i v_i}{2V_q\epsilon_0 c n_i}, \tag{5}$$

$I_p$ is the pump intensity, $c$ is the speed of light in the vacuum, $a_i^{\dagger}$ is the creation operator of mode $i$, $V_q$ is the quantization volume, and $n_i$ and $v_i$ are the refractive index and the group velocity of mode $i$, respectively. $A_p(x,y)$ is the transverse spatial distribution of the pump which is dimensionless and has a maximum value of unity. The temporal part of the electric fields is accounted for in Fermi's golden rule; therefore, only the spatial part of the fields is considered. Combining Eqs. (3) and (4), we obtain

$$\hat{H}^{(n)} = \gamma^{(n)} f(\Delta k^{(n)})\prod_{i}^{n}\sqrt{c_i}a_i^{\dagger} + \text{H.c.}, \tag{6}$$

where

$$\gamma^{(n)} = -\frac{n!\chi^{(n)}}{2^n}\sqrt{\frac{2I_p\epsilon_0}{cn_p}}, \tag{7}$$

$f(\Delta k^{(n)})$, which we will call the phase-matching function, is given by

$$f(\Delta k^{(n)}) = \int F(\vec{r})A_p(x,y)e^{\imath\,\Delta\vec{k}^{(n)}\cdot\vec{r}}d^3\vec{r}, \tag{8}$$

and

$$\Delta\vec{k}^{(n)} = \vec{k}_p - \sum_{i}^{n}\vec{k}_i \tag{9}$$

is the wave-vector mismatch. The phase-matching function is of importance as it couples all modes involved in the interaction together. From Eq. (1), the rate of transition from the vacuum state to a $n$-photon state is

$$\Gamma^{(n)} = \frac{2\pi}{\hbar^2}[\gamma^{(n)}]^2 D(\Delta\vec{k}^{(n)}, \Delta\omega^{(n)})\prod_{i=1}^{n}|c_i|, \tag{10}$$

where

$$D(\Delta\vec{k}^{(n)}, \Delta\omega^{(n)}) = |f(\Delta k^{(n)})|^2\delta(\Delta\omega^{(n)}). \tag{11}$$

Equation (10) gives the rate of transition into a single set of $n$ modes. The total transition rate is given by the number of transitions in the interval between $\vec{k}_i$ and $\vec{k}_i + d\vec{k}_i$. In three-dimensional wave-vector space each state occupies a $k$-space volume of $\frac{(2\pi)^3}{V_q}$. Therefore, the transition rate to a $n$th-order state in the intervals $d\vec{k}_i$ is

$$dN^{(n)} = \Gamma^{(n)}\frac{V_q^n}{(2\pi)^{3n}}\prod_{i=1}^{n}d\vec{k}_i, \tag{12}$$

which gives

$$dN^{(n)} = \frac{2\pi}{\hbar^2}[\gamma^{(n)}]^2 D(\Delta\vec{k}^{(n)}, \Delta\omega^{(n)})\frac{V_q^n}{(2\pi)^{3n}}\prod_{i=1}^{n}|c_i|d\vec{k}_i. \tag{13}$$

A significant feature of Eq. (13) is the dependence on $\hbar$. Each factor of $c_i$ scales with $\hbar$, which, in turn, leads to $dN^{(n)}$ scaling as $\hbar^{n-2}$.

## III. PHASE-MATCHING FUNCTION

The phase-matching function and the energy conservation form a distribution $D(\Delta\vec{k}^{(n)}, \Delta\omega^{(n)})$ that limits the number of available final states in which the initial state can transition. The shape of the distribution dictates the spectral properties and the degree of entanglement of the generated photons. The energy conservation term due to the nearly instantaneous response of $n$th-order SPDC is given by a $\delta$ function following from Fermi's golden rule. The phase-matching term, given by

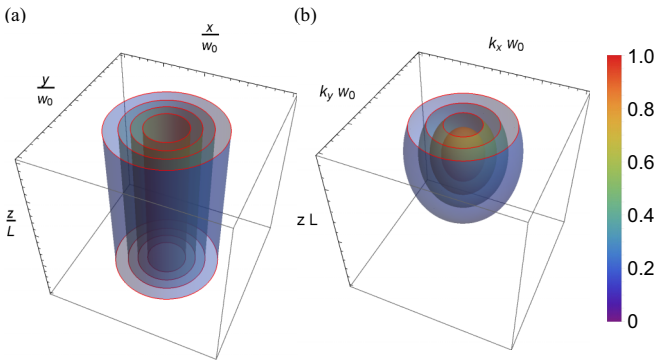


FIG. 1. The distributions of (a) the interaction volume in which the nonlinear process takes place and (b) the phase-matching function in the reciprocal ($k$) space.

Eq. (8), can be normalized by defining the interaction volume as $V = \int F(\vec{r})A_p(x,y)d\vec{r}$. Then,

$$|f(\Delta\vec{k}^{(n)})|^2 = |\mathcal{F}[F(\vec{r})A_p(x,y)]|^2 \equiv |\tilde{f}(\Delta\vec{k}^{(n)})|^2 V, \quad (14)$$

where $\mathcal{F}$ denotes the Fourier transform. The function $|\tilde{f}(\Delta k^{(n)})|^2$ is constant and dimensionless when integrated over all $k$ spaces.

We assume the pump to be a Gaussian beam with the waist $w_0$,

$$A_p(x,y) = \exp\left(-\left[\frac{x^2+y^2}{w_0^2}\right]\right), \quad (15)$$

and a Rayleigh length much longer than the length $L$ of the nonlinear medium. If the spatial distribution of the susceptibility is uniform throughout the medium, then

$$F(\vec{r}) = \Pi\left(\frac{z}{L}\right), \quad (16)$$

where $\Pi$ is a rectangular function. Such a distribution is shown in Fig. 1(a). From Eqs. (14)–(16), the squared modulus of the normalized phase-matching function is

$$|\tilde{f}(\Delta\vec{k}^{(n)})|^2 = V\ \exp\left(-\frac{\Delta k_x^2+\Delta k_y^2}{2}w_0^2\right)\mathrm{sinc}^2\left(\frac{\Delta k_z L}{2}\right), \quad (17)$$

which is shown in Fig. 1(b).

As mentioned before, when integrated over all $k$ spaces, this function is a dimensionless constant. For this reason, whenever a convolution with a broader function is considered, we will replace Eq. (17) with

$$|\tilde{f}(\Delta\vec{k}^{(n)})|^2 \to (2\pi)^3\delta^{(3)}(\Delta\vec{k}^{(n)}). \quad (18)$$

Further on, we will distinguish between two detection regimes. The first is when the detection bandwidth $D_i$ is broader than the phase-matching function $V^{-1}$. This we will refer to as the broadband regime. The second is when the detection bandwidth is narrower than the phase-matching function. This we will call the narrow-band regime. In the broadband regime, without loss of generality, we will use Eq. (18) to represent the phase-matching function, and in the narrow-band case, we will use Eq. (17).

## IV. COMPARISON OF HIGH-ORDER PROCESSES TO LOW-ORDER PROCESSES

Unlike second-order SPDC where the final states are well defined by energy and momentum conservation, the final states of higher-order SPDC are almost continuous in $k$ space as the number of ways to fulfill the phase-matching condition increases with the process order $n$. In this situation, the number of states that can be registered are limited by the detection scheme. For this reason, we will treat the broadband and narrow-band regimes as two separate problems. For both detection regimes, we find the rates of $(n-1)$-photon generation via a $n$th-order process and a $(n-1)$-order process and derive a relationship between these rates.

### A. Broadband detection

Integrating Eq. (13) over all wave vectors captured by the detection bandwidths $D_i$ gives the $(n-1)$-photon flux into $(n-1)$-detector bandwidths,

$$N_{n-1}^{(n)} = \frac{2\pi}{\hbar^2}[\gamma^{(n)}]^2\frac{V_q^n}{(2\pi)^{3(n-1)}}V\int_{D_1}\cdots\int_{D_{n-1}}\int_{-\infty}^{\infty}\delta(\Delta\vec{k}^{(n)}) \times \delta(\Delta\omega^{(n)})\prod_{i=1}^{n}|c_i|d\vec{k}_i. \quad (19)$$

The ratio of $(n-1)$-photon generation rates via a $n$th-order process and a $(n-1)$-order process is given by

$$\frac{N_{n-1}^{(n)}}{N_{n-1}^{(n-1)}} = \frac{n^2}{32\pi^3}\frac{[\chi^{(n)}]^2}{[\chi^{(n-1)}]^2}\langle E_{bb}^2\rangle, \quad (20)$$

where we introduce the squared effective broadband vacuum field [26] as

$$\langle E_{bb}^2\rangle = \frac{\hbar}{2\epsilon_0 c}\int_{-\infty}^{\infty}\frac{\omega_n v_n}{n_n}\xi(\vec{k}_n)d\vec{k}_n, \quad (21)$$

where the reduced phase-matching function,

$$\xi(\vec{k}_n) = \frac{\displaystyle\int_{D_1}\cdots\int_{D_{n-1}}\delta(\Delta\vec{k}^{(n)})\delta(\Delta\omega^{(n)})\prod_{i=1}^{n-1}|c_i|d\vec{k}_i}{\displaystyle\int_{D_1}\cdots\int_{D_{n-1}}\delta(\Delta\vec{k}^{(n-1)})\delta(\Delta\omega^{(n-1)})\prod_{i=1}^{n-1}|c_i|d\vec{k}_i} \quad (22)$$

accounts for the increased number of ways to fulfill the phase-matching condition with $n$ modes. The effective broadband vacuum field is the total electric field of all photons in mode $\vec{k}_n$ that satisfy the reduced phase-matching condition.

### B. Narrow-band detection

The rate of $(n-1)$-photon generation into $n-1$ narrow detection intervals $D_i$ is

$$\Delta N_{n-1}^{(n)} = \frac{2\pi}{\hbar^2}[\gamma^{(n)}]^2\frac{V_q^n}{(2\pi)^{3n}}\int_{-\infty}^{\infty}D(\Delta\vec{k}^{(n)},\Delta\omega^{(n)})|c_n|d\vec{k}_n \times\prod_{i=1}^{n-1}|c_i|D_i. \quad (23)$$

The ratio of the $(n-1)$-photon generation rate for a $n$th-order process and a $(n-1)$-order process is

$$\frac{\Delta N_{n-1}^{(n)}}{\Delta N_{n-1}^{(n-1)}} = \frac{n^2}{32\pi^3}\frac{[\chi^{(n)}]^2}{[\chi^{(n-1)}]^2}\langle E_{nb}^2\rangle, \tag{24}$$

where we define the squared effective narrow-band vacuum field as

$$\langle E_{nb}^2\rangle = \frac{\hbar}{2\epsilon_0 c V^2}\int_{-\infty}^{\infty}\frac{\omega_n v_n}{n_n}|f(\Delta\vec{k}^{(n)})|^2 d\vec{k}_n \tag{25}$$

assuming that the $(n-1)$-order process is exactly phase matched and the $n$th-order process satisfies energy conservation.

Approximating the nonlinear susceptibility as $\chi^{(n)} \approx E_a^{-n}$, where $E_a$ is the atomic field strength [27], one finds that the ratio of the effective vacuum field and atomic field gives the reduction in efficiency from a high-order process to the next lower-order process,

$$\frac{N_{n-1}^{(n)}}{N_{n-1}^{(n-1)}} = \frac{n^2}{32\pi^3}\frac{\langle E_{bb}^2\rangle}{E_a^2}, \tag{26}$$

$$\frac{\Delta N_{n-1}^{(n)}}{\Delta N_{n-1}^{(n-1)}} = \frac{n^2}{32\pi^3}\frac{\langle E_{nb}^2\rangle}{E_a^2}. \tag{27}$$

## V. SEEDING

In this section, we move from the spontaneous generation of photons via $n$th-order SPDC to the case where we stimulate the process using a coherent seed beam. We assume that the seed has a wave-vector $\vec{k}_s = \vec{k}_n$ and a frequency $\omega_s = \omega_n$. If the seed has a high intensity, then a classical field description is adequate. The Hamiltonian of a seeded process is therefore

$$\hat{H}_s^{(n)} = \gamma_s^{(n)} f_s(\Delta\vec{k}^{(n)})(\iota)^{n-1}\prod_i^{n-1}\sqrt{c_i}a_i^\dagger + \text{H.c.}, \tag{28}$$

where [28]

$$\gamma_s^{(n)} = -\frac{n!\chi^{(n)}}{2^n}\sqrt{\frac{4I_sI_p}{c^2 n_p n_s}}, \tag{29}$$

$I_s$ is the seed intensity and the phase-matching function in the seeded case is

$$f_s(\Delta\vec{k}^{(n)}) = \int F(\vec{r})A_p(x,y)A_s(x,y)e^{\iota\,\Delta\vec{k}\cdot\vec{r}}d^3\vec{r}, \tag{30}$$

where $A_s(x,y)$ is the transverse field distribution of the seed beam.

The seeded $n$th-order Hamiltonian (28) contains $(n-1)$-photon creation operators. This means that the characteristics of $n$-photon emission are lost and the photon statistics become similar to that of $(n-1)$-photon SPDC.

The rate of transition to a $(n-1)$-photon state is

$$\Gamma_s^{(n)} = \frac{2\pi}{\hbar^2}\left[\gamma_s^{(n)}\right]^2 D(\Delta\vec{k}^{(n)},\Delta\omega^{(n)})\prod_i^{n-1}|c_i|, \tag{31}$$

which gives the rate of transition into the intervals $d\vec{k}_i$,

$$dN_{s,n-1}^{(n)} = \frac{2\pi}{\hbar^2}\left[\gamma_s^{(n)}\right]^2 D(\Delta\vec{k}^{(n)},\Delta\omega^{(n)})\frac{V_q^{n-1}}{(2\pi)^{3(n-1)}}\prod_{i=1}^{n-1}|c_i|d\vec{k}_i. \tag{32}$$

### A. Broadband detection

The seeded $(n-1)$-photon emission rate in the broadband case is

$$N_{s,n-1}^{(n)} = \frac{2\pi}{\hbar^2}\left[\gamma_s^{(n)}\right]^2\frac{V_q^{n-1}}{(2\pi)^{3(n-1)}}\int_{D_1}\cdots\int_{D_{n-1}} D(\Delta\vec{k}^{(n)},\Delta\omega^{(n)}) \times\prod_{i=1}^{n-1}|c_i|d\vec{k}_i. \tag{33}$$

By taking the ratio of Eqs. (19) and (33) we obtain

$$\frac{N_{s,n-1}^{(n)}}{N_{n-1}^{(n)}} = \frac{|E_s|^2}{\langle E_{bb}^2\rangle}, \tag{34}$$

where the squared seed field amplitude is

$$|E_s|^2 = \frac{2I_s}{\epsilon_0 n_s c}. \tag{35}$$

### B. Narrow-band detection

The seeded $(n-1)$-photon emission rate into $(n-1)$-narrow-band detectors with bandwidths $D_i$ is

$$\Delta N s_{n-1}^{(n)} = \frac{2\pi}{\hbar^2}\left[\gamma_s^{(n)}\right]^2\frac{V_q^{n-1}}{(2\pi)^{3(n-1)}}D(\Delta\vec{k}^{(n)},\Delta\omega^{(n)})\prod_{i=1}^{n-1}|c_i|D_i. \tag{36}$$

The ratio of the $(n-1)$-photon emission rate into $(n-1)$ detectors for a seeded and unseeded $n$th-order process is

$$\frac{\Delta N s_{n-1}^{(n)}}{\Delta N_{n-1}^{(n)}} = \frac{|E_s|^2}{\langle E_{nb}^2\rangle}. \tag{37}$$

In both broadband and narrow-band cases, the use of a seed has an advantage only if the seed field is larger than the corresponding effective vacuum field.

In the broadband case, if the reduced phase-matching function $|\xi(\vec{k}_n)|$ is broad, then the effective field is comparatively large. Using a continuous-wave (cw) seed would require too high intensities to overcome the effective broadband vacuum field strength. In this situation it is advantageous to work with tightly focused pulsed seed and pump. The product of the seed and pump peak intensities averaged over time and space yields a factor of inverse duty cycle and area, significantly enhancing the efficiency of the $n$th-order process. For the seed to be used optimally, one must overlap the pump and seed waves in space and time. This follows from the phase-matching function Eq. (30), which is given by the convolution of the seed and pump. There are drawbacks to using pulsed sources and tightly focused beams. Other nonlinear effects, that also scale as the product of strong classical fields, begin to compete with seeded TOPDC. In particular, the Kerr effect will change

the phase-matching conditions adding an extra term to $\Delta k$. Although we do not consider such effects, they are worth noting. In addition, using tightly focused beams limits the nonlinear interaction length.

## VI. EFFICIENCY OF UNSEEDED TOPDC

Here, we consider the case of $n = 3$, which corresponds to TOPDC. We estimate the photon emission rates for both seeded and unseeded TOPDC in rutile ($TiO_2$), which has been suggested previously as potentially efficient for TOPDC [29].

From Eq. (13), the differential generation rate of a three-photon state via TOPDC into modes $k_1$, $k_2$, and $k_3$ is

$$\mathcal{N}(\vec{k}_1,\vec{k}_2,\vec{k}_3) = \frac{dN^{(3)}}{d\vec{k}_1 d\vec{k}_2 d\vec{k}_3} = R^{(3)}\frac{\omega_1\omega_2\omega_3 v_1 v_2 v_3}{n_1 n_2 n_3}|\tilde{f}(\Delta\vec{k}^{(3)})|^2 \times \delta(\Delta\omega^{(3)}), \tag{38}$$

where

$$R^{(3)} = \frac{\hbar V}{8(2\pi)^8\epsilon_0^3 c^3}[\gamma^{(3)}]^2. \tag{39}$$

Again we consider the cases of: (1) broadband detection and (2) narrow-band detection. In both situations, we can choose to detect the rate of triple photons in modes $k_1$, $k_2$, and $k_3$, the rate of double photons in modes $k_1, k_2$ or the rate of single photons in mode $k_1$. For double- and single-photon count rates Eq. (38) is integrated over all wave vectors of the unregistered mode (mode 3).

### A. Broadband detection of TOPDC

Following from Sec. III, the phase-matching function in Eq. (38) can be replaced by a $\delta$ function. Calculating the integrals,

$$N_3 = \int_{D_1}\int_{D_2}\int_{D_3}\mathcal{N}(\vec{k}_1,\vec{k}_2,\vec{k}_3)d\vec{k}_1 d\vec{k}_2 d\vec{k}_3, \tag{40a}$$

$$N_2 = \int_{-\infty}^{+\infty}\int_{D_2}\int_{D3}\mathcal{N}(\vec{k}_1,\vec{k}_2,\vec{k}_3)d\vec{k}_1 d\vec{k}_2 d\vec{k}_3, \tag{40b}$$

$$N_1 = \int_{-\infty}^{+\infty}\int_{-\infty}^{+\infty}\int_{D_3}\mathcal{N}(\vec{k}_1,\vec{k}_2,\vec{k}_3)d\vec{k}_1 d\vec{k}_2 d\vec{k}_3 \tag{40c}$$

gives the triple-photon, double-photon, and single-photon fluxes into three-, two-, and one-broadband detectors whose bandwidths are given by $D_1$, $D_2$, and $D_3$.

### B. Narrow-band detection of TOPDC

The phase-matching function in Eq. (38) is replaced by Eq. (17) in the narrow-band regime. The triple-, double-, and single-photon fluxes into three-, two-, and one-narrow-band detector(s) are given by

$$\Delta N_3 = \mathcal{N}(\vec{k}_{01},\vec{k}_{02},\vec{k}_{03})D_1 D_2 D_3, \tag{41a}$$

$$\Delta N_2 = \int_{-\infty}^{+\infty}\mathcal{N}(\vec{k}_1,\vec{k}_{02},\vec{k}_{03})d\vec{k}_1 D_2 D_3, \tag{41b}$$

$$\Delta N_1 = \int_{-\infty}^{+\infty}\int_{-\infty}^{+\infty}\mathcal{N}(\vec{k}_1,\vec{k}_2,\vec{k}_{03})d\vec{k}_1 d\vec{k}_2 D_3, \tag{41c}$$

where $D_1$, $D_2$, and $D_3$ are the detector bandwidths centered around modes $\vec{k}_{01}$, $\vec{k}_{02}$, and $\vec{k}_{03}$.

In practice, integration over all unregistered wave vectors is impossible as dispersion information only exists for a limited bandwidth. In the calculations below, we integrate over a range of wave vectors where dispersion relation for $TiO_2$ still holds true, which results in an *underestimation* of the total photon flux. The deviation from the true emission rate is comparatively small due to the factor $\omega_1\omega_1\omega_3$ in Eq. (38), which implies that near-degenerate frequencies contribute more than nondegenerate frequencies. An additional source of error is introduced by assuming the cubic susceptibility is fixed at an effective value, independent of frequency. This, in general, is not true, however $TiO_2$ is optically transparent over the frequencies we consider, and the nonlinear susceptibility changes by only 2% with a fixed pump [30].

From now on, we choose to work in frequency-angle variables $(\omega,\theta,\phi)$ as opposed to wave-vector space $(\vec{k})$, the transformation is given in the Appendix. The parameter [see Eq. (38)],

$$\int_{-\infty}^{+\infty}\int_{-\infty}^{+\infty}\mathcal{N}(\vec{k}_1,\vec{k}_2,\vec{k}_3)d\vec{k}_1 d\vec{k}_2 = (2\pi)^4 R^{(3)}\frac{\omega_3 v_3}{c^2 n_3}\int\frac{\tilde{\omega}_1(\theta_2,\vec{k}_3)\tilde{\omega}_2^3(\theta_2,\vec{k}_3)\tilde{v}_1\tilde{n}_2}{\tilde{n}_1^2}\sin(\theta_2)d\theta_2 \tag{42}$$

is common to both the narrow-band and broadband single-photon emission rates and gives information on the spread and spectral content of the photons emitted. The frequency $\tilde{\omega}_1(\theta_2,\vec{k}_3)$ is given by Eq. (A5) and $\tilde{v}_1,\tilde{n}_1$ are the group and refractive index evaluated at $\tilde{\omega}_1(\theta_2,\vec{k}_3)$. The frequency $\tilde{\omega}_2(\theta_2,\vec{k}_3)$ is given in Eq. (A10), $\tilde{n}_2$ is the refractive index evaluated at this frequency, and $\theta_2$ is the polar angle of mode 2.

A key point in all further calculations is finding the dependence $\tilde{\omega}_2(\theta_2,\vec{k}_3)$ at fixed $\vec{k}_3$ (assuming azimuthal symmetry). This dependence, which we will refer to as the frequency-angle contour of mode 2, gives all the points $\omega_2,\theta_2$ that satisfy conditions $\Delta\vec{k}^{(3)} = 0$, $\Delta\omega^{(3)} = 0$ at fixed $\vec{k}_3$. An example is plotted in Fig. 2 for TOPDC in $TiO_2$ assuming the pump wavelength to be $\lambda_p = 532$ nm and mode 3 parameters fixed to collinear degenerate case: $\lambda_3 = 1596$ nm, $\theta_3 = 0^\circ$.

Phase matching is satisfied using the birefringence present in $TiO_2$ crystals. Type-I phase matching (o $\rightarrow$ eee) is assumed. Varying the angle subtended by the optic axis of the crystal and the pump propagation direction, further called the crystal orientation, it is possible to change the shape of the frequency-angle contour as shown in Fig. 2.

The value of Eq. (42) and by extension the single-photon flux scales as the *length* of the frequency-angle contour. How

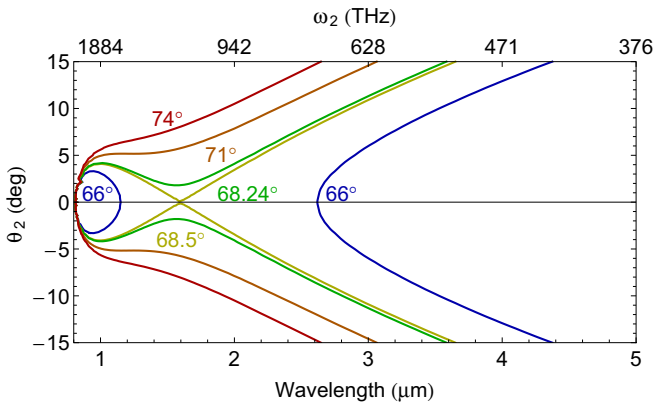


FIG. 2. Frequency-angle contour for a $TiO_2$ crystal with type-I (o → eee) phase matching at different orientation angles. The pump wavelength is $\lambda_p = 532$ nm, and the parameters for mode 3 are fixed at $\lambda_3 = 1596$ nm and $\theta_3 = 0°$.

the single-photon differential rate [Eq. (42)] changes with the crystal orientation is plotted in Fig. 3. The highest rate occurs at the crystal orientation 68.24°, corresponding to a contour that crosses the collinear degenerate point; hence for all subsequent calculations, this orientation was considered. The discontinuity in Fig. 3 is due to the fact that we describe the phase-matching function as a $\delta$ function multiplied by a constant width $L^{-1}$. At the crossing point of degenerate phase matching (see Fig. 2), the phase-matching width does not scale as $L^{-1}$ but as $L^{-1/2}$. Hence the assumption that the phase-matching width is constant is incorrect in this small interval where degenerate phase matching occurs.

Plotting the integrated value of the frequency-angular contour as a function of the mode 3 parameters gives the frequency-angle spectrum of the single-photon emission from unseeded TOPDC, shown in Fig. 4. The resulting spectrum is very broad compared to the equivalent spectrum for SPDC. This is expected in TOPDC due to the increased number of degrees of freedom in which to satisfy phase matching. In fact, we expect this trend to continue when looking at higher orders of SPDC. Nevertheless, the TOPDC spectrum is not uniform, and, for a fixed frequency, it does not span all angles.

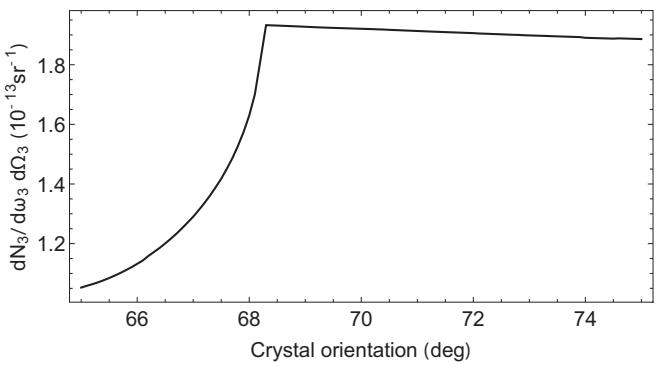


FIG. 3. The differential single-photon count rate for TOPDC in a 5-mm $TiO_2$ crystal pumped by 100 mW as a function of the crystal orientation angle. The pump wavelength is $\lambda_p = 532$ nm, and the parameters for mode 3 are $\lambda_3 = 1596$ nm and $\theta_3 = 0°$.

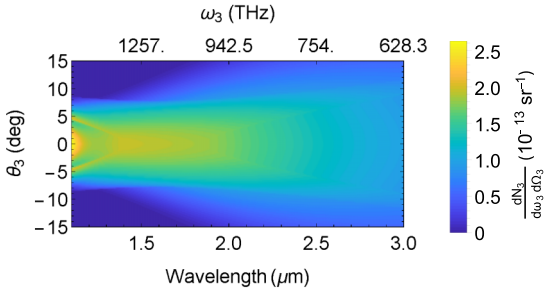


FIG. 4. The frequency-angle spectrum of the single-photon differential generation rate in mode 3 for unseeded TOPDC in a $TiO_2$ crystal oriented at 68.24°. The crystal length is $L = 5$ mm, and the pump power is $P_p = 100$ mW.

It follows from Eq. (40c) that integration over a region of the spectrum shown in Fig. 4 with the limits set by $D_3$ gives the total single-emission rate $N_1$ for the broadband case.

## VII. EFFICIENCY OF SINGLY SEEDED TOPDC

From the general consideration of Sec. V, singly seeded TOPDC results in the emission of photon pairs, similar to two-photon SPDC. This is a consequence of fixing one of the final states in TOPDC. In this case, we fix mode 3 such that $\vec{k}_3 = \vec{k}_s$. From Eq. (32), the differential rate of two-photon transitions via seeded TOPDC is

$$\mathcal{N}_s = \frac{dN_s^{(3)}}{d\vec{k}_1 d\vec{k}_2} = R_s^{(3)} \frac{\omega_1 \omega_2 v_1 v_2}{n_1 n_2} \left|\tilde{f}\left(\Delta\vec{k}_s^{(3)}\right)\right|^2 \delta\left(\Delta\omega_s^{(3)}\right), \quad (43)$$

where

$$R_s^{(3)} = \frac{V}{4(2\pi)^5 \epsilon_0^2 c^2} \left[\gamma_s^{(3)}\right]^2. \quad (44)$$

### A. Broadband detection of seeded TOPDC

Equations (40) and (41) are simplified as seeded TOPDC only generates pair states; hence, we are limited to detecting just photon pairs and single photons. The rate of two-photon and single-photon states collected by two and one detectors, respectively, is

$$N_{s,2} = \int_{D_1}\int_{D_2} \mathcal{N}_s(\vec{k}_1, \vec{k}_2) d\vec{k}_1 d\vec{k}_2, \quad (45a)$$

$$N_{s,1} = \int_{D_1}\int_{-\infty}^{+\infty} \mathcal{N}_s(\vec{k}_1, \vec{k}_2) d\vec{k}_1 d\vec{k}_2. \quad (45b)$$

### B. Narrow-band detection of seeded TOPDC

The rate of double- and single-photon emissions into narrow-bands $D_2$ and $D_1$ is

$$\Delta N_{s,2} = \mathcal{N}_s(\vec{k}_{01}, \vec{k}_{02}) D_1 D_2, \quad (46a)$$

$$\Delta N_{s,1} = \int_{-\infty}^{+\infty} \mathcal{N}_s(\vec{k}_1, \vec{k}_{02}) d\vec{k}_1 D_2, \quad (46b)$$

where $\vec{k}_{01}$ and $\vec{k}_{02}$ represent the central wave vectors of the detection bands $D_2$ and $D_1$.

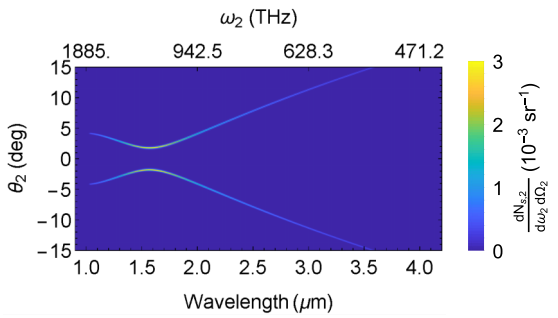


FIG. 5. The frequency-angle spectrum of mode 2 for seeded TOPDC in $TiO_2$ of length $L = 5$ mm for the pump power $P_p = 100$ mW and the crystal orientation 68.5°.

The seeded analog of Eq. (42) is

$$\int_{-\infty}^{+\infty} \mathcal{N}_s(\vec{k}_1, \vec{k}_2) d\vec{k}_1 = 2\pi R_s^{(3)} V \frac{\tilde{\omega}_1^3 \omega_2 n_1 v_2}{n_2} \times \exp\left(-\frac{\Delta k_x^2 + \Delta k_y^2}{4} w_0^2\right) \times \mathrm{sinc}^2\left(\frac{\Delta k_z L}{2}\right), \quad (47)$$

which, again, is common to both the single-broadband and the single-narrow-band seeded transition rates. For the sake of completeness we assume that the phase-matching function can be broader than $D_1$, hence in Eq. (47), the phase-matching function is given by Eq. (17).

The differential single-photon emission rate is plotted in Fig. 5 as a function of the frequency, wavelength, and angle of emission in mode 2. The first noticeable feature is that the frequency-angle spectrum resembles the one typically observed in SPDC. This follows from our earlier statement that seeding a $n$th-order process reduces the $n$th-order Hamiltonian to a $(n-1)$-order Hamiltonian. The second is that, when $\vec{k}_3 = \vec{k}_s$, the frequency-angle contour given by $\tilde{\omega}_2(\Omega_2, \vec{k}_s)$ is similar to the spectrum in Fig. 5. The difference between the two cases is that the frequency-angle spectrum has a nonzero width due to the nonzero width of the phase-matching function. A significant point is that the integrated values of both the frequency-angular contour in Fig. 4 and the frequency-angular spectrum in Fig. 5 over all frequencies and angle spaces are equivalent. Comparing the frequency-angle spectrum of seeded TOPDC in Fig. 5 and the equivalent spectrum for spontaneous TOPDC shows that the seeded spectrum is far more concentrated to particular regions. This is advantageous especially in the narrow-band case as it is clear where to place detectors to collect the largest number of single photons. Conversely the TOPDC spectrum is broad and uniform over a large region of the angular frequency spectrum, making it harder to distinguish from background sources of light.

Comparing Eq. (42) for spontaneous TOPDC and Eq. (47) for seeded TOPDC reveals that the reduced Planck constant enters only Eq. (42) through $R^{(3)}$ and is absent from Eq. (47). It is also absent for the equivalent relations for SPDC. This, along with other effects, such as a non-Gaussian Wigner function [9,10], implies that spontaneous TOPDC displays quantum features that are not observed in either seeded TOPDC or SPDC. More generally, it follows from Eq. (13) that SPDC of order $n$ contains the Planck constant to the power $n-2$ as mentioned previously.

## VIII. NUMERICAL ESTIMATIONS OF SEEDED AND UNSEEDED PHOTON COUNT RATES

In this section, we take into account the available experimental parameters, including the quantum efficiencies $\eta_{1-3}$ for the three detectors, and estimate the count rates for triple coincidences $\eta_1\eta_2\eta_3 N_3$, double coincidences $\eta_1\eta_2 N_2$, and single-photon counts $\eta_1 N_1$ from unseeded TOPDC in both the broadband regime and the narrow-band regime. The quantum efficiencies are assumed to be independent of frequency or angle. We take the effective cubic susceptibility for the type-I process in $TiO_2$ to be $\chi^{(3)} = 2.1 \times 10^{-20}$ m$^2$ V$^{-2}$ [27], the length $L = 5$ mm and the orientation angle 68.24° (see Fig. 3). For spontaneous TOPDC, we assume a cw pump with power $P_p = 100$ mW. For seeded TOPDC, we assume a pulsed pump and seed (see Sec. V) overlapped with a beam-waist $w_0 = 100$ $\mu$m and duty cycle $\mathcal{D} = 2 \times 10^{-8}$. The seed has mean power $P_s = 10$ mW and the pump $P_p = 100$ mW which corresponds to peak intensities of $I_s = 1.6 \times 10^{13}$ and $I_p = 1.6 \times 10^{14}$ W m$^{-2}$, respectively. The seed wavelength is assumed to be 1620 nm, slightly redshifted from the detection bandwidth.

### A. Broadband detection

Broadband detection refers to both frequency and angle. In this situation, the best strategy is using multimode avalanche photodiodes (APDs) [31]. Despite their lower quantum efficiency compared to superconducting nanowires, they are more efficient to use due to the larger collection angle. For such a situation, we assume a quantum efficiency of 15% over a frequency range of 1200–1600 nm. The capture angle is limited only by the aperture size of the emission collected which, for arguments' sake, we limit to −10° to 10°.

Figure 6(a) shows the expected triple coincidence, double coincidence, and single count rates via seeded and unseeded TOPDC in $TiO_2$. Without seeding, it is feasible to observe single counts and double coincidences, whose rates are 33 and 1 Hz, respectively. The estimated triple-coincidence rate is on the order of a few per hour and, after taking into account the dark counts of the detectors (4 kHz), would be very difficult to measure.

The seed enhances the detection rate of single and double photons by roughly $10^7$ times compared to the case of unseeded TOPDC, although this comes at the cost of losing the three-photon state. The seeded two-photon emission rate is 300 kHz. However, this would be difficult to measure experimentally with the duty cycle assumed, which would require a low repetition rate. It is therefore more reasonable to reduce the mean powers of the pump and seed pulses so that the repetition rate of the laser is much larger than the two-photon emission rate. Despite this, with such rates, one can readily study the properties of the three-photon state generated via spontaneous TOPDC by using methods, such as stimulated emission tomography.

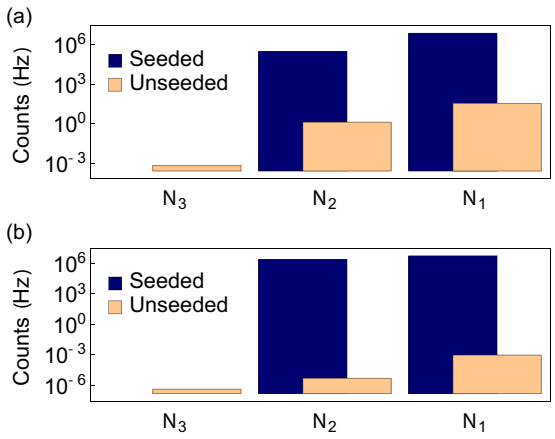


FIG. 6. The expected triple-, double-, and single-photon count rates of seeded and unseeded TOPDC in 5-nm $TiO_2$ for (a) the broadband regime and (b) the narrow-band regime. The seed beam is centered at 1620 nm, the pump power is $P_p = 100$ mW, and the overlapped seed peak intensity $I_s = 1.6 \times 10^{13}$ W m$^{-2}$. The count rates calculated for the broadband regime assume collection of wavelengths from 1200 to 1600 nm and angles from $-10^\circ$ to $10^\circ$ with a detection efficiency of 15%. The count rates for the narrow-band regime assume collection of wavelengths from 1579 to 1589 nm and angles from $-0.25^\circ$ to $0.25^\circ$ with a detection efficiency of 80%.

### B. Narrow-band detection

Working in the narrow-band detection regime is advantageous if fluorescence or other sources of noise are competing processes. By choosing a bandwidth where the three-photon emission is particularly strong, one can maximize the signal-to-noise ratio (SNR). Emission rates around the degeneracy frequency are relatively high due to the factor $\omega_1\omega_2\omega_3$ that appears in Eq. (10). For a 100-$\mu$m beam waist, single-mode superconducting nanowire detectors capture angles between $-0.25^\circ$ and $0.25^\circ$ with a quantum efficiency of 80%. In addition to this, the number of dark counts for superconducting nanowires can be as low as 50 Hz as opposed to multimode APDs where the dark counts are around 4 kHz. This further increases the SNR for the narrow-band regime. We assume that the frequency bandwidth is restricted to $1584 \pm 5$ nm, which is close to degeneracy but satisfies the frequency matching in the seeded case.

The calculated narrow-band triple-, double-, and single-photon count rates are compared in Fig. 6(b). Here the rates are lower than in the broadband case, but the seed provides a stronger enhancement. This is expected as seeding fixes one of the triplet modes thereby reducing the number of degrees of freedom; it follows that photons are emitted into a fewer number of modes, but the count rate per mode increases. The number of photon double counts from seeded TOPDC is roughly $3 \times 10^6$ Hz, which as mentioned previously can only be measured with a suitably fast laser repetition rate. For comparison, the number of SPDC photon pairs generated from potassium titanyl phosphate pumped by a 100-mW pump centered on 532 nm with a 10-nm bandpass collection is $1.6 \times 10^9$ Hz [32].

## IX. CONCLUSION

In conclusion, we have derived a general expression for the emission rate of $n$th-order SPDC. The phase-matching and energy conservation conditions can be written as a single function $D(\Delta\vec{k}^{(n)}, \Delta\omega^{(n)})$, which restricts the frequency-angle distribution. As the function $D(\Delta\vec{k}^{(n)}, \Delta\omega^{(n)})$ restricts only two degrees of freedom, the angular spectrum of two-photon SPDC is fully defined. However, moving to higher-order SPDC, the number of degrees of freedom exceeds the restrictions set by $D(\Delta\vec{k}^{(n)}, \Delta\omega^{(n)})$ leading to broader angular spectra with increasing $n$.

Calculations are simplified by distinguishing between two regimes with broadband and narrow-band collections of $n$-photon radiation. In the broadband regime, the width of the distribution $D(\Delta\vec{k}^{(n)}, \Delta\omega^{(n)})$ is irrelevant as only the integrated distribution matters. As such, the TOPDC efficiency does not depend on the width of the frequency-angular spectrum (see Figs. 5 and 2) for modes 1 and 2, only the length of the curve. In the narrow-band case, $D(\Delta\vec{k}^{(n)}, \Delta\omega^{(n)})$ is evaluated at the central position of the detector bandwidths.

By comparing the rate of $(n-1)$-photon state generation for a $n$th-order process and a $(n-1)$-order process, one can conveniently define an effective field that describes the total electric field of all phase-matched states. We show that the ratio of this effective field squared and the atomic field squared roughly gives the reduction in efficiency from one process to the next.

The rate of emission for $n$th-order SPDC scales as $\hbar^{n-2}$. Scaling with the Planck constant is a feature commonly attributed to quantum characteristics. As such, all high-order SPDC states are very much distinguished from the two-photon state generated from two-photon SPDC. This is in agreement with the fact that these processes produce non-Gaussian states whereas the output state of second-order SPDC without post-selection is Gaussian.

Coherently seeding one of the modes that satisfies phase matching maps the $n$th-order nonlinear Hamiltonian to a $(n-1)$-order Hamiltonian. As a result, the photon statistics of a $n$th-order seeded process mimic those of a $(n-1)$-order process. Moreover, using a seed gives an enhancement to the rate of photon emission, equal to the ratio of the seed field amplitude squared and the effective squared vacuum field. When working in the pulsed regime, one uses the peak seed field amplitude, hence there can be a large enhancement using a seed.

Finally, for the particular case of TOPDC ($n = 3$) we have estimated the photon emission rates for rutile. We show that despite being far broader than the typical second-order SPDC spectrum, the distribution $D(\Delta\vec{k}^{(n)}, \Delta\omega^{(n)})$ still limits the angular spectrum of TOPDC. Plotting the distribution over frequency and angle reveals optimum regions in which to collect single, double, and triplet photons.

Optical fibers, planar waveguides, and whispering gallery resonators [12,33,34] have all been suggested as promising platforms on which to generate triplet states via TOPDC. Although we have concentrated on bulk materials here, seeding may also be implemented for each of the aforementioned methods. However, in most cases, the phase matching in fibers, planar waveguides, and whispering gallery resonators

is satisfied by modal overlap. Hence there is a slight modification on the theoretical approach outlined in this paper to calculate the number of photon triplets, doubles, and singles.

The estimated triplet rates are too low to readily observe, however we show that by utilizing a pulsed seed beam one can greatly improve the rate of emission. From the estimates, the seed gives an enhancement of roughly $10^9$ in the broadband case and $10^{14}$ in the narrow-band case. The drawback is that one can only observe double-photon counts in the seeded regime and statistics predicted for the three-photon state cannot be acquired. Despite this, using stimulated tomography one can reconstruct the statistics of the three-photon state [23].

## ACKNOWLEDGMENTS

We acknowledge the financial support by Deutsche Forschungsgemeinschaft (DFG) (Grants No. CH-1591/3-1 and No. JO-1090/3-1). We would like to thank Alfred U'Ren and Karina Garay-Palmett for the useful discussions we had with them.

## APPENDIX: DERIVATION OF EMISSION RATES FOR UNSEEDED TOPDC

The integrals,

$$\int_{-\infty}^{+\infty} \mathcal{N}(\vec{k}_1,\vec{k}_2)d\vec{k}_1, \tag{A1a}$$

$$\int_{-\infty}^{+\infty}\int_{-\infty}^{+\infty} \mathcal{N}(\vec{k}_1,\vec{k}_2)d\vec{k}_1\, d\vec{k}_2 \tag{A1b}$$

can be solved analytically. As the integration domain is broader than the phase-matching function, we can replace $|\tilde{f}(\Delta k^{(n)})|^2$ with (18), which gives

$$\int_{-\infty}^{+\infty} \mathcal{N}(\vec{k}_1,\vec{k}_2)d\vec{k}_1 = (2\pi)^3 R^{(3)} \int \frac{\omega_1\omega_2\omega_3 v_1 v_2 v_3}{n_1 n_2 n_3}\delta(\Delta\vec{k}^{(3)}) \times \delta(\Delta\omega^{(3)})d\vec{k}_1. \tag{A2}$$

The frequency is related to the wave vector as

$$\frac{n(\omega_i)\omega_i}{c} = \sqrt{k_{ix}^2 + k_{iy}^2 + k_{iz}^2}, \tag{A3}$$

where $n(\omega_i)$ is the dispersion dependence. Then, integration in Eq. (A2) gives

$$\int_{-\infty}^{+\infty} \mathcal{N}(\vec{k}_1,\vec{k}_2)\, d\vec{k}_1 = (2\pi)^3 R^{(3)} \frac{\tilde{\omega}_1(\vec{k}_2,\vec{k}_3)\omega_2\omega_3\tilde{v}_1 v_2 v_3}{\tilde{n}_1 n_2 n_3} \times \delta[\omega_p - \tilde{\omega}_1(\vec{k}_2,\vec{k}_3) - \omega_2 - \omega_3], \tag{A4}$$

where $\tilde{\omega}_1(\vec{k}_2,\vec{k}_3)$ is found from the equation,

$$\left[\frac{n(\tilde{\omega}_1(\vec{k}_2,\vec{k}_3))\tilde{\omega}_1(\vec{k}_2,\vec{k}_3)}{c}\right]^2 = (k_{2x}+k_{3x})^2 + (k_{2y}+k_{3y})^2 + (k_{2z}+k_{3z}-k_p)^2, \tag{A5}$$

and $\tilde{n}_1, \tilde{v}_1$ are the refractive index and group velocity at this frequency (both functions of $\vec{k}_2, \vec{k}_3$).

Finding the expression for the single-photon generation rate requires integrating Eq. (A4) in $\vec{k}_2$. It is now convenient to pass from the wave-vector space to the frequency-angle space, hence we use the following transformations to substitute into Eq. (A5):

$$k_{ix} = \frac{n_i\omega_i}{c}\sin\theta_i\cos\phi_i, \tag{A6a}$$

$$k_{iy} = \frac{n_i\omega_i}{c}\sin\theta_i\sin\phi_i, \tag{A6b}$$

$$k_{iz} = \frac{n_i\omega_i}{c}\cos\theta_i. \tag{A6c}$$

The differential $d\vec{k}_i$ is then,

$$d\vec{k}_i = \frac{n_i^2\omega_i^2}{c^2 v_i} d\omega_i d\Omega_i, \tag{A7}$$

where the solid angle interval is

$$d\Omega_i = \sin(\theta_i)d\theta_i d\phi_i. \tag{A8}$$

By assuming azimuthal symmetry, we can rewrite Eq. (A5) as

$$n^2(\tilde{\omega}_1(\vec{k}_2,\vec{k}_3))\tilde{\omega}_1^2(\vec{k}_2,\vec{k}_3) = (n_2\omega_2\sin\theta_2 + n_3\omega_3\sin\theta_3)^2 + (n_2\omega_2\cos\theta_2 + n_3\omega_3\cos\theta_3 - n_p\omega_p)^2. \tag{A9}$$

Due to the azimuthal symmetry, integration of Eq. (A4) in $d\phi_2$ results in a factor of $2\pi$. Integration in $\omega_2$ fixes it to be

$$\tilde{\omega}_2(\omega_3,\theta_2,\theta_3) = \omega_p - \tilde{\omega}_1(\tilde{\omega}_2,\omega_3,\theta_2,\theta_3) - \omega_3. \tag{A10}$$

Obtaining the analytical expression for $\tilde{\omega}_2$ is difficult; therefore, in all calculations, we solve Eq. (A10) numerically or graphically. As a result,

$$\int_{-\infty}^{+\infty}\int_{-\infty}^{+\infty} \mathcal{N}\, d\vec{k}_1 d\vec{k}_2 = (2\pi)^4 R^{(3)}\frac{\omega_3 v_3}{c^2 n_3}\int \frac{\tilde{\omega}_1(\tilde{\omega}_2,\omega_3,\theta_2,\theta_3)\tilde{\omega}_2^3(\omega_3,\theta_2,\theta_3)\tilde{v}_1\tilde{n}_2}{\tilde{n}_1^2} \times \sin\theta_2 d\theta_2. \tag{A11}$$

To find the rate of photon emission within a certain detection bandwidth $\Delta\omega_{\text{det}}$ in the frequency and $\Delta\Omega_{\text{det}}$ in the solid angle, one should additionally integrate the differential rate (A11) over these bandwidths.

[1] S. Harris, M. Oshman, and R. Byer, Observation of Tunable Optical Parametric Fluorescence, Phys. Rev. Lett. **18**, 732 (1967).

[2] D. Magde and H. Mahr, Study in Ammonium Dihydrogen Phosphate of Spontaneous Parametric Interaction Tunable from 4400 to 16 000 Å, Phys. Rev. Lett. **18**, 905 (1967).

[3] S. Akhmanov, V. Fadeev, R. Khokhlov, and O. Chunaev, Quantum noise in parametric light amplifiers, ZhETF Pisma Redaktsiiu **6**, 575 (1967).

[4] R. E. Slusher, L. W. Hollberg, B. Yurke, J. C. Mertz, and J. F. Valley, Observation of Squeezed States Generated by

Four-Wave Mixing in an Optical Cavity, Phys. Rev. Lett. **55**, 2409 (1985).

[5] C. K. Hong and L. Mandel, Experimental Realization of a Localized One-Photon State, Phys. Rev. Lett. **56**, 58 (1986).

[6] J. Rarity, P. Tapster, and E. Jakeman, Observation of sub-poissonian light in parametric downconversion, Opt. Commun. **62**, 201 (1987).

[7] L.-A. Wu, H. J. Kimble, J. L. Hall, and H. Wu, Generation of Squeezed States by Parametric Down Conversion, Phys. Rev. Lett. **57**, 2520 (1986).

[8] A. Heidmann, R. J. Horowicz, S. Reynaud, E. Giacobino, C. Fabre, and G. Camy, Observation of Quantum Noise Reduction on Twin Laser Beams, Phys. Rev. Lett. **59**, 2555 (1987).

[9] K. Banaszek and P. L. Knight, Quantum interference in three-photon down-conversion, Phys. Rev. A **55**, 2368 (1997).

[10] P. Elyutin and D. Klyshko, Three-photon squeezing: exploding solutions and possible experiments, Phys. Lett. A **149**, 241 (1990).

[11] T. Felbinger, S. Schiller, and J. Mlynek, Oscillation and Generation of Nonclassical States in Three-Photon Down-Conversion, Phys. Rev. Lett. **80**, 492 (1998).

[12] M. Corona, K. Garay-Palmett, and A. B. U'Ren, Experimental proposal for the generation of entangled photon triplets by third-order spontaneous parametric downconversion in optical fibers, Opt. Lett. **36**, 190 (2011).

[13] E. A. Rojas González, A. Borne, B. Boulanger, J. A. Levenson, and K. Bencheikh, Continuous-Variable Triple-Photon States Quantum Entanglement, Phys. Rev. Lett. **120**, 043601 (2018).

[14] K. Bencheikh, F. Gravier, J. Douady, A. Levenson, and B. Boulanger, Triple photons: a challenge in nonlinear and quantum optics, C. R. Phys. **8**, 206 (2007).

[15] M. G. Moebius, F. Herrera, S. Griesse-Nascimento, O. Reshef, C. C. Evans, G. G. Guerreschi, A. Aspuru-Guzik, and E. Mazur, Efficient photon triplet generation in integrated nanophotonic waveguides, Opt. Express **24**, 9932 (2016).

[16] M. Akbari and A. Kalachev, Third-order spontaneous parametric down-conversion in a ring microcavity, Laser Phys. Lett. **13**, 115204 (2016).

[17] A. Cavanna, F. Just, X. Jiang, G. Leuchs, M. V. Chekhova, P. S. J. Russell, and N. Y. Joly, Hybrid photonic-crystal fiber for single-mode phase matched generation of third harmonic and photon triplets, Optica **3**, 952 (2016).

[18] H. Hübel, D. R. Hamel, A. Fedrizzi, S. Ramelow, K. J. Resch, and T. Jennewein, Direct generation of photon triplets using cascaded photon-pair sources, Nature (London) **466**, 601 (2010).

[19] P. J. Mosley, J. S. Lundeen, B. J. Smith, P. Wasylczyk, A. B. U'Ren, C. Silberhorn, and I. A. Walmsley, Heralded Generation of Ultrafast Single Photons in Pure Quantum States, Phys. Rev. Lett. **100**, 133601 (2008).

[20] M. Khoshnegar, T. Huber, A. Predojević, D. Dalacu, M. Prilmüller, J. Lapointe, X. Wu, P. Tamarat, B. Lounis, P. Poole, G. Weihs, and H. Majedi, A solid state source of photon triplets based on quantum dot molecules, Nat. Commun. **8**, 15716 (2017).

[21] N. C. Menicucci, P. van Loock, M. Gu, C. Weedbrook, T. C. Ralph, and M. A. Nielsen, Universal Quantum Computation with Continuous-Variable Cluster States, Phys. Rev. Lett. **97**, 110501 (2006).

[22] J. Douady and B. Boulanger, Experimental demonstration of a pure third-order optical parametric downconversion process, Opt. Lett. **29**, 2794 (2004).

[23] M. Liscidini and J. E. Sipe, Stimulated Emission Tomography, Phys. Rev. Lett. **111**, 193602 (2013).

[24] D. N. Klyshko, *Photons Nonlinear Optics* (Gordon & Breach, Philadelphia, 1988), Chap. 6, pp. 286–298.

[25] D. J. Griffiths, *Introduction to Electrodynamics*, 3rd ed. (Prentice Hall, Upper Saddle River, NJ, 1962).

[26] M. V. Chekhova, O. A. Ivanova, V. Berardi, and A. Garuccio, Spectral properties of three-photon entangled states generated via three-photon parametric down-conversion in a $\chi^{(3)}$ medium, Phys. Rev. A **72**, 023818 (2005).

[27] R. W. Boyd, *Nonlinear Optics* (Academic, Burlington, MA, 2003).

[28] Dimensionality of $\gamma_s^{(n)}$ and $\gamma^{(n)}$ is not the same as $\gamma_s^{(n)}$ accounts for the classical seed field amplitude, whereas $\gamma^{(n)}$ does not.

[29] N. Borshchevskaya, K. Katamadze, S. Kulik, and M. Fedorov, Three-photon generation by means of third-order spontaneous parametric down-conversion in bulk crystals, Laser Phys. Lett. **12**, 115404 (2015).

[30] A. Borne, P. Segonds, B. Boulanger, C. Félix, and J. Debray, Refractive indices, phase-matching directions and third order nonlinear coefficients of rutile $TiO_2$ from third harmonic generation, Opt. Mater. Express **2**, 1797 (2012).

[31] Id220 infrared single-photon detector, https://www.idquantique.com/single-photon-systems/products/id220/.

[32] M. Fiorentino, S. M. Spillane, R. G. Beausoleil, T. D. Roberts, P. Battle, and M. W. Munro, Spontaneous parametric down-conversion in periodically poled KTP waveguides and bulk crystals, Opt. Express **15**, 7479 (2007).

[33] S. Krapick, B. Brecht, H. Herrmann, V. Quiring, and C. Silberhorn, On-chip generation of photon-triplet states, Opt. Express **24**, 2836 (2016).

[34] D. V. Strekalov, C. Marquardt, A. B. Matsko, H. G. Schwefel, and G. Leuchs, Nonlinear and quantum optics with whispering gallery resonators, J. Opt. **18**, 123002 (2016).